Scientific Visualization, 2025, volume 17, number 3, pages 35 - 48, DOI: 10.26583/sv.17.3.04

Physics-Guided Machine Learning for Predicting Gas Permeability of Standard Carbonate Core Plugs from Low-Resolution Microtomography Image Stacks

R. I. Kadyrov[1], T. H. Nguyen[2], E. O. Statsenko[3]
Kazan Federal University (Institute of Geology and Petroleum Technologies), Kazan, Russia
[1] ORCID: 0000-0002-7566-6312, rail7777@gmail.com
[2] ORCID: 0000-0001-6155-9017, thanhtu154@gmail.com
[3] ORCID: 0000-0001-6259-1713, e.statsenko@yahoo.com

Abstract

This study presents a physics-guided workflow for predicting the gas permeability of carbonate reservoirs directly from low-resolution microtomography (μCT) imagery. Standard core plugs were scanned at 34.6–36 μm/voxel, and a total of 52,327 grayscale d aggregation against experimental plug-scale measurements. The grayscale images and log-transformed permeability labels were used to train a Swin Transformer model, pre-trained on ImageNet. Two models were developed independently: one using harmonic-mean aggregation and the other using the bottleneck approach. Both models demonstrate stable convergence despite the highly skewed data distribution. The harmonic-mean model achieved $R^2 = 0.904$ on the validation set, while the bottleneck model yielded $R^2 = 0.879$. Although the higher R^2 reflects a closer fit to the overall trend, the bottleneck model, in blind testing on ten independent samples (0.4–2300 μm² × 10^{-3}), reduced the MAE from 165 to 104 μm² × 10^{-3} (–37 %) and the RMSE from 255 to 140 μm² × 10^{-3} (–45 %) relative to the harmonic-mean model. The method provides a fast and interpretable permeability prediction based solely on raw μCT slices, without requiring image segmentation or 3D reconstruction. The proposed approach demonstrates robust performance across a wide range of standard carbonate plugs and effectively captures permeability trends even in the presence of structural heterogeneity. While samples with extremely large fractures or vugs can introduce local inconsistencies in labelling due to the limitations of slice-based estimation, these cases are rare and can be systematically addressed in future work. Overall, the results highlight the strong potential of physics-guided machine learning to accelerate digital core analysis and provide reliable, image-driven permeability predictions for complex carbonate reservoirs.

Keywords: permeability, carbonates, μCT, digital core, porous structure, standard core plug, physics-guided machine learning, 2D image analysis.

1. Introduction

Determining the reservoir properties of rocks, such as porosity and absolute permeability, is essential for the development of oil and gas fields and for enhancing oil recovery [1]. The evaluation of these properties can be challenging due to the heterogeneity and complexity of rock structures, which vary significantly across different geological formations and burial histories [2,3]. In particular, permeability, being one of the most fundamental physical characteristics of porous materials, is largely governed by the pore space structure [4–6].

Currently, three main approaches can be distinguished for estimating the permeability of reservoir rocks: experimental measurements, empirical models, and digital rock physics. Experimental measurements are performed on standard core samples and require significant time, labor, and financial resources [7]. There are also empirical and theoretical models, in-

cluding the well-known Kozeny–Carman equation, which link porosity, permeability, and other reservoir properties [8,9]. Although these empirical models are efficient and cost-effective, their universality is often limited, necessitating parameter adjustments for different rock types and specific structural features [10]. Reservoir properties can also be assessed through numerical simulations; however, these methods require the reconstruction of three-dimensional (3D) pore networks, which demands substantial computational resources and introduces hidden uncertainties, including resolution loss and structural distortions [11]. Moreover, the results of numerical simulations are often difficult to correlate with experimental data due to discrepancies in sample sizes [6,12], especially in highly heterogeneous reservoirs such as carbonates [13].

Machine learning offers an alternative for estimating reservoir properties. Techniques such as X-ray computed microtomography (μCT) enable the acquisition of images of the internal structure of porous media, which serve as input data for machine learning algorithms [14]. Machine learning and deep learning methods can predict rock properties from images within seconds and with minimal computational costs [1,14,15]. This offers significant advantages over experimental measurements and numerical simulations, which are not efficient for processing multiple samples simultaneously. Several studies have successfully demonstrated the potential to predict porosity and permeability based on images. For example, deep learning has been applied to estimate permeability from high-resolution 2D thin section images, showing high accuracy and fast processing [16]. It has also been shown that physics-guided models can predict the permeability of synthetic 2D porous media with high accuracy and orders of magnitude faster than traditional simulations, including cases where classical empirical equations are ineffective [17]. Convolutional neural networks (CNNs) have been used to estimate porosity from Berea sandstone images, both with and without segmentation [18], demonstrating good agreement with experimental data [19]. It was also shown that CNNs can successfully work with raw grayscale microtomographic images. In [20], both shallow and deep learning methods were applied to 3D microtomographic data for permeability prediction in comparison with numerical simulations: deep networks outperformed gradient boosting and linear regression, and machine learning methods demonstrated significant computational speed advantages over direct simulations based on the lattice Boltzmann method.

Despite this progress, machine learning models face challenges when transferring to new datasets due to overfitting and the limited number of training examples. This is particularly relevant when working with 3D data, which requires substantial computational resources. A promising approach is to divide the 3D volume into stacks of 2D slices and train models on this set of images [12,14]. This method works especially well for porosity prediction; however, estimating permeability presents additional challenges due to its strong nonlinear dependence on the 3D pore geometry, connectivity, and flow pathways. To overcome these limitations, attempts have been made to link rock properties extracted from 2D images to the 3D structure. In [17], it was demonstrated that a physics-guided convolutional neural network, trained on numerical filtration data using the lattice Boltzmann method, can quickly and accurately estimate the 2D permeability of synthetic porous media images. In [21], porosity and absolute permeability of carbonate core plugs were predicted based on statistical 2D pore features extracted from stacks of high-resolution microtomographic slices (0.8 – 14 μm) using watershed-based pore segmentation. The final property values were determined by an ensemble meta-model that combined predictions from several independent machine learning models. Another approach [22] involved analytically estimating the permeability of porous media from high-resolution 2D images, combining the Kozeny–Carman equation with fractal theory. This method enables permeability calculation without 3D pore structure reconstruction, using pore space parameters extracted from 2D slices, and demonstrated good agreement with numerical simulation results based on the lattice Boltzmann method.

However, these approaches have several limitations. Some focus on predicting 2D permeability, which complicates their application to the assessment of filtration properties in real 3D samples. Model verification is often conducted using numerical simulation data rather

than experimental measurements. The use of high-resolution images (up to a few microns) limits the size of the analyzed samples, which is especially critical for carbonates with pronounced heterogeneity and the need to satisfy representativeness conditions. Additionally, these approaches require significant effort in data preparation — segmentation, feature extraction, as well as subsequent meta-model training or complex analytical calculations.

In this study we propose a hybrid workflow that couples low-resolution μCT imaging (voxel size 34.6–36 μm) with machine-learning inference to rapidly estimate plug-scale gas permeability of standard carbonate cores from stacks of raw 2D slices. The main idea is to use empirical calculations to train a machine learning model to predict 3D permeability from individual microtomographic slices without segmentation and then use the distribution of these predictions across the stack to estimate the permeability of the entire sample.

2. Materials and methods

2.1. μCT scanning of core plugs

A collection of 71 standard carbonate samples (cylinders with a height and diameter of 30 mm) was prepared for this study. It is important to note that samples exhibiting pronounced caverns or fracturing were excluded from the dataset, as the presence of such secondary features complicates the correct application of the selected approach, which is primarily focused on matrix porosity.

The samples were scanned using the General Electric Phoenix v|tome|x S 240 microfocus and nanofocus X-ray computed tomography system with a resolution of 34.6–36.0 μm. The following scanning parameters were used: X-ray tube current — 150 μA, voltage — 150 kV, number of projections — 1200, averaging factor — 3, and exposure time — 200 ms per projection.

The acquired projections were reconstructed into 3D images using the phoenix datos|x software. To eliminate edge artifacts and to standardize the data, a cylindrical region of interest (ROI) of 737×737 voxels in diameter and height was selected for all samples, ensuring that the ROI was fully contained within the boundaries of each standard core plug. The resulting 3D volume was then converted into a stack of 2D slices along the z-axis, which coincides with the axis of the cylinder, yielding 737 images per stack (Fig. 1).

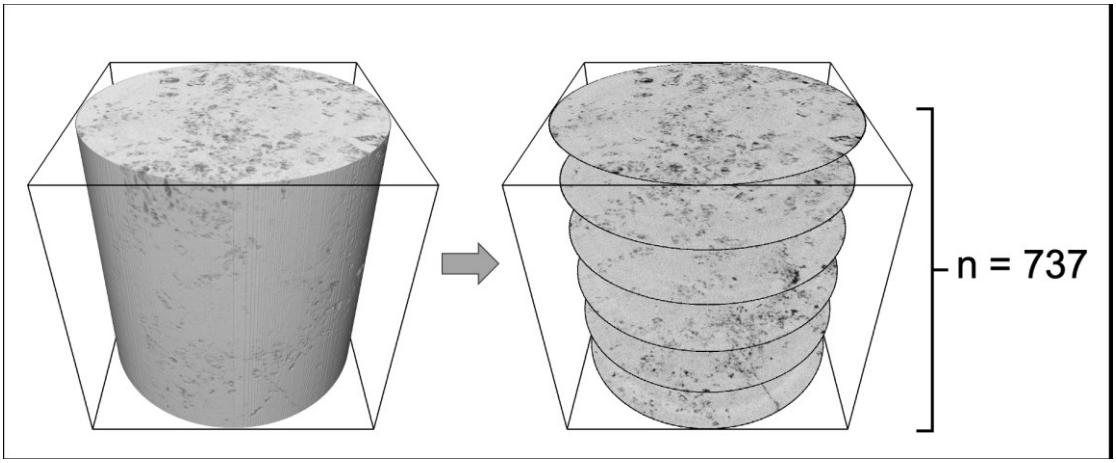

Fig. 1. Low-resolution μCT workflow: 737 axial slices extracted from a 30 mm carbonate core plug after cylindrical masking

2.2. Experimental measurements

The open porosity and gas permeability with Klinkenberg correction for each sample were measured using the PIK-PP gas permeability and porosity analyzer (Russia). The permeability distribution across the sample collection ranges from 0.1 to 2192 $\mu m^2 \times 10^{-3}$, reflecting the

high heterogeneity of the studied carbonate samples. In the combined boxplot (Fig.2) the open-porosity distribution is compact: the median is 9.3 %, the inter-quartile range spans only ~6–13 %, and fewer than 5 % of samples exceed 20 %, so porosity varies modestly around a low-to-moderate mean. Permeability, by contrast, is highly skewed. One quarter of the measurements sit at the detection limit of 0.1 $\mu m^2 \times 10^{-3}$, yet the box already stretches to a median of 7 $\mu m^2 \times 10^{-3}$ and an upper quartile of ~115 $\mu m^2 \times 10^{-3}$, while the upper whisker and outliers run beyond 1,100 $\mu m^2 \times 10^{-3}$. If the analysis is restricted to slices with permeability > 1 $\mu m^2 \times 10^{-3}$ (≈65 % of the data), most values cluster between 10 and 200 $\mu m^2 \times 10^{-3}$ and only a handful of samples rise above 1,000 $\mu m^2 \times 10^{-3}$, confirming that flow capacity is far more heterogeneous than pore volume across the studied plugs.

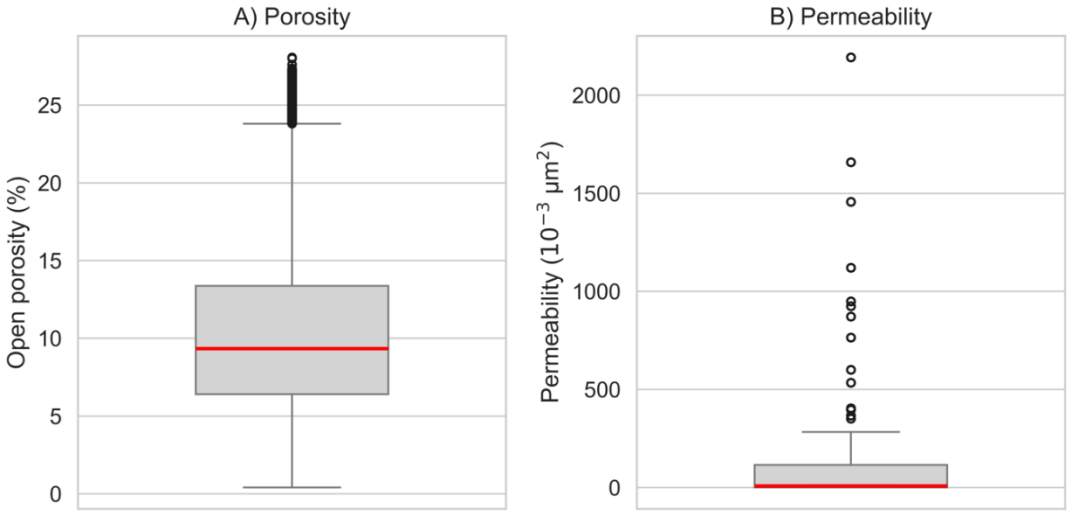

Fig. 2. Boxplot of open porosity (%) and permeability (10^{-3} μm^2) across 71 carbonate core plugs; red lines mark the medians

2.3. Image Labeling

A key step in building a physics-guided model is the creation of reliable and representative labeling that reflects the internal filtration heterogeneity of the core sample. When machine learning is applied to 2D slices, it is necessary to ensure the correct matching of each image with a value that represents permeability. To address this challenge, this study implemented an approach based on a fractal model [22], according to which the permeability of a porous medium can be approximately estimated from 2D images using geometric characteristics of the pore space, such as porosity, minimum and maximum pore radii, tortuosity, and fractal dimension.

A previous study [14] demonstrated that when using microtomographic images with a resolution of 38 μm, machine learning models are capable of extracting key structural features of carbonate rocks with sufficient accuracy, despite the limited spatial resolution and the presence of unresolved pores.

The foundation of this model is a pore space segmentation method, in which the pore boundaries are individually selected for each sample so that the average 2D porosity across the stack matches the experimentally measured 3D porosity. This ensures consideration of unresolved pores and adapts the segmentation procedure to the specific characteristics of each sample.

On the resulting segmented 2D images, pore boundaries were determined using the watershed algorithm [23], after which the maximum pore radius r_{max} in the plane was calculated for each pore region using the distance transform algorithm [21]. Additionally, the two-dimensional fractal dimension of the entire segmented pore structure was calculated using the box counting method [24].

Since the spatial resolution of the microtomographic images in this study is limited (34.6–36 μm), determining the minimum pore radius r_{min} is challenging. Numerous studies have shown that the minimum pore radii observed on 2D slices of carbonate rocks are typically less than 1 μm [25,26]. Therefore, to standardize calculations and account for unresolved pores, an approximate minimum pore radius of r_{min} = 1 μm was assumed for all images in this study.

Subsequently, based on the analytical approach proposed in [22], the key parameters of the 3D pore space were sequentially calculated for each segmented image. In this process, the bulk porosity was assumed to be equal to the porosity of the image:

$$\varphi_{3D} = \varphi_{2D} \tag{1}$$

After this, the transformation dimension parameter D_T is calculated, which reflects the change in the nature of pore space filling when transitioning from area to volume.

$$D_T = \left[\frac{(5-4D_T)\ln(\varphi_{3D})}{\ln\left(\frac{r_{min}}{r_{max}}\right)} + 1\right] + \left\langle \frac{(5-4D_T)\ln(\varphi_{3D})}{\ln\left(\frac{r_{min}}{r_{max}}\right)} \times \left\{ \frac{\log\left[3-\frac{(5-4D_T)\ln(\varphi_{3D})}{\ln(\frac{r_{min}}{r_{max}})}\right]}{\log(\varphi_{3D})} - \frac{\log\left[2-\frac{(5-4D_T)\ln(\varphi_{3D})}{\ln(\frac{r_{min}}{r_{max}})}\right]}{\log(\varphi_{3D})} \right\} \right\rangle \tag{2}$$

In cases where the value of D_T exceeded 1.125, it was limited to 1.124999 to avoid violating the physical interpretation of the model (for example, inversion where $r_{3D,min} > r_{3D,max}$ [22].

Subsequently, based on the transformation dimension parameter D_T, the porosity value φ_{3D}, and the ratio of pore radii r_{min} and r_{max} on the 2D slices, the three-dimensional fractal dimension D_f was calculated:

$$D_f = 3 - \frac{(5-4D_T)\ln(\varphi_{3D})}{\ln(r_{min}/r_{max})} \tag{3}$$

The next step is to calculate the volume of the sample within which the pore space characteristics are evaluated:

$$V = \left\{ \frac{\pi D_f r_{max}^{3-D_T} (2r_{max})^{\frac{(4D_T-4)(3-D_T)}{5-4D_T}}}{4\varphi_{3D}(3-D_T-D_f)} \left[1 - \left(\frac{r_{min}}{r_{max}}\right)^{\frac{3-D_T-D_f}{5-4D_T}}\right] \right\}^{\frac{3(5-4D_T)}{3-D_T}}. \tag{4}$$

Next, the maximum $r_{3D,max}$ and minimum ($r_{3D,min}$) pore radii in the 3D space are calculated:

$$r_{3D,max} = \frac{r_{max}}{\left[\sqrt[3]{V}/(2r_{max})\right]^{\frac{4D_T-4}{5-4D_T}}};\ r_{3D,min} = \frac{r_{min}}{\left[\sqrt[3]{V}/(2r_{min})\right]^{\frac{4D_T-4}{5-4D_T}}}. \tag{5}$$

Finally, using the calculated parameters for the 3D space, the 3D permeability is determined:

$$K_{3D} = \frac{\pi D_f 2^{D_T} r_{3D,max}^{D_f} (r_{3D,max}^{3-D_f+D_T} - r_{3D,min}^{3-D_f+D_T}}{16V^{\frac{1+D_T}{3}}(3-D_f+D_T)} \tag{6}$$

Thus, an individual 3D permeability value was calculated for each image in the stack, resulting in 737 such values per sample. Although the low resolution and pore shape distortions during segmentation may lead to discrepancies between the calculated and experimental values, the resulting distribution of 3D permeabilities along the axis of the cylindrical sample clearly demonstrates the internal filtration heterogeneity of the sample.

2.4. Aggregation and normalization

At the previous stage, 737 individual permeability values were obtained for each sample—one for every 2D slice in the stack. However, to train a model that can be directly compared with experimental measurements, these data must be reduced to a single value representing the permeability of the entire sample. The most universal and potentially accurate solution would be to build a meta-model trained on the known experimental values together with the local slice-wise predictions; such a model could automatically learn the optimal aggregation transformation. Unfortunately, the limited number of experimentally characterised samples in the available data set makes this approach impractical without a high risk of overfitting.

To convert the distributed set of slice-based 3D permeability values into a single estimate for the whole core, two approaches were tested. The first relies on the harmonic mean, which is widely used in porous-media flow problems when zones with different permeability are connected in series along the flow direction—as is the case for vertical flow through a cylindrical core.

In this model, the lowest-permeability intervals dominate the overall flow resistance, so the harmonic mean is the most appropriate averaging method for estimating the effective permeability of a vertical stack. The harmonic mean is calculated as follows:

$$K_{harm} = \frac{N}{\sum_{i=1}^{N} \frac{1}{K_{3D}(i)}}, \quad (7)$$

where $K_{3D}(i)$ is the 3D permeability value at the i-th slice, and N = 737 is the total number of images in the stack.

Using this formula yields an averaged permeability that is physically equivalent to the total resistance encountered by a filtration flow passing through sequential layers of varying permeability. This approach requires no additional parameters or calibration and serves as a baseline aggregation method.

The second method is based on the bottleneck concept, which assumes that the overall permeability of a porous medium is controlled by the lowest-permeability zones that restrict flow. This is particularly relevant for heterogeneous carbonate rocks, where even a brief constriction in a pore channel can markedly reduce the effective permeability of the entire sample.

To implement this method, the stack of 737 slices was analyzed with a sliding window five slices wide, which diminishes the impact of random outliers or segmentation errors. Within each window the arithmetic mean of the 3D-permeability values was calculated, and the minimum of all such window means was then taken:

$$k_b(i) = \frac{1}{\omega} \sum_{j=i}^{i+\omega-1} K_{3D}(j), \; i = 1, \dots, N - \omega + 1 \quad (8)$$

$$K_{\text{bottle}} = \min_{i=1}^{N-\omega+1} k_b(i) \quad (9)$$

where $K_{3D}(i)$ is the 3-D permeability at slice i, w = 5 is the window width, and N = 737 is the total number of slices in the stack.

After computing the slice-wise 3D permeabilities, it was necessary to adjust their scale so they could be compared with the experimental data. For each core we obtained 737 local values $K_{3D}(i)$ and one experimentally measured permeability K_{exp}. Aggregating the local values with either the harmonic mean or the bottleneck model yields an integral permeability estimate, but because the slice-wise calculations are approximate these estimates can systematically deviate from the experimental measurement.

To eliminate this discrepancy, a normalization procedure was applied. This involved scaling all local permeability values by a constant coefficient C, determined individually for each aggregation method. For the harmonic-mean approach the normalization coefficient C_{harm} was chosen so that the harmonic mean of the scaled permeabilities matched the experimental value exactly:

$$K_{exp} = \frac{N}{\sum_{i=1}^{N} \frac{1}{C_{harm} \cdot K_{3D}(i)}} \quad (10)$$

which gives the expression:

$$C_{harm} = \frac{K_{exp}}{N} \sum_{i=1}^{N} \frac{1}{K_{3D}(i)}. \quad (11)$$

For the bottleneck model, the coefficient C_{bottle} was determined so that the minimum mean permeability across a sliding window of width ω = 5 slices, after normalization, matched K_{exp}:

$$K_{exp} = \min_{i=1,\dots,N-\omega+1} \frac{1}{\omega} \sum_{j=i}^{i+\omega-1} C_{bottle} \cdot K_{3D}(j), \quad (12)$$

from which:

$$C_{bottle} = \frac{\omega K_{exp}}{\min_{i=1,\dots,N-\omega+1} \sum_{j=i}^{i+\omega-1} K_{3D}(j)}. \quad (13)$$

The application of this normalization preserved the shape of the permeability distribution along the stack while ensuring that the aggregated predictions matched the actual experimental values. As a result, each 2D image in the stack was assigned a normalized 3D permeability value, completing the labeling process. Two independent datasets were thus created: one based on harmonic mean aggregation and the other on the bottleneck model.

2.5. Model architecture for permeability prediction

To solve the task of predicting permeability from μCT images we employed the Swin Transformer architecture [27]. Unlike conventional convolutional neural networks (CNNs), the Swin Transformer uses a self-attention mechanism to model both local and global dependencies within an image. The architecture is hierarchical: the image is split into small windows in which local self-attention is applied, and window shifting then enables interaction between neighboring regions (Fig.3). This structure allows the network to capture fine-scale pore details and long-range relationships across the entire image simultaneously.

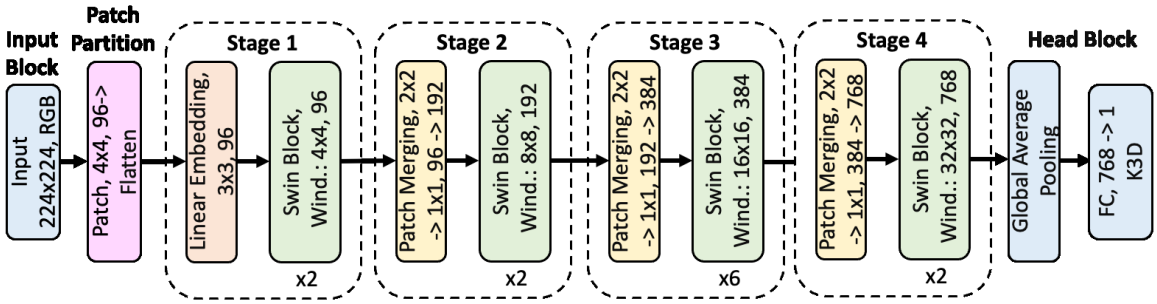

Fig. 3. Swin Transformer model architecture used for the gas permeability prediction on slices

To reduce the impact of the limited data volume, the network was trained with weights pre-trained on ImageNet-1k. During data preparation all 16-bit μCT images were intensity-normalized, masked along the cylindrical outline, and then resized to 224 × 224 pixels using area interpolation. Additional data augmentation was applied by randomly rotating the images by 0°, 90°, 180° and 270°, which improved the model's generalization ability.

Two separate Swin Transformer models were trained. The first used a data set in which permeability values were aggregated with the harmonic mean, while the second used a data set based on the bottleneck model. In each case the data set contained 52,327 images of carbonate samples (71 cores × 737 slices). Each image was assigned a training label equal to the normalized 3D permeability value.

Because the 3D permeability values span several orders of magnitude, the training set had a highly skewed distribution. To stabilize learning and handle both small and large values correctly, the models were trained on the logarithms of permeability. The regression target was therefore the log permeability; at inference the predictions were transformed back to physical units by exponentiation.

Each data set was split 80 % / 20 % into training and validation subsets. Training used the AdamW optimizer with an initial learning rate of 1×10^{-4}, a batch size of 16, and ran for 20 epochs. The loss function was the mean squared error (MSE) between the predicted and true log permeability. The mean absolute error (MAE) and coefficient of determination (R^2) were also monitored on the validation set.

The network followed the standard hierarchical Swin Transformer design with progressive resolution reduction and feature-dimension expansion at each stage. After all layers, the output features were passed through global average pooling and a fully connected regression head that outputs a single scalar value. ReLU activations and a Dropout layer were used to improve generalization.

Training was carried out in PyTorch 1.13.1 on an NVIDIA Quadro P5000 GPU with CUDA 11.7 under Windows 10, using Python 3.8.

3. Results and discussion

3.1. Model Training Results

To solve the task of predicting normalized 3D permeability values from microtomographic images, two separate Swin Transformer models were trained: one on a dataset formed using harmonic mean aggregation of permeability, and the other on a dataset based on the bottleneck model (Fig.4). Both models were trained for 20 epochs on a dataset of 52,327 images (41,861 for training and 10,466 for validation).

The harmonic mean model demonstrated high convergence and training stability. By the end of training, the logarithmic loss value decreased to 0.0715 on the training set and 0.1596 on the validation set. The final metrics in log-space were as follows: mean squared error (MSE) – 0.1596, mean absolute error (MAE) – 0.1912, coefficient of determination (R^2) – 0.988. The low error values are attributed to the use of logarithmic transformation of permeability, which helped smooth the data range and ensure stable model convergence. In physical scale, the coefficient of determination was $R^2 = 0.904$, indicating a high degree of agreement between the predicted and measured permeability values.

The bottleneck model also demonstrated good convergence and training stability, reaching a loss value of 0.0474 in log-scale on the training set and 0.0642 on the validation set by epoch 20. The main performance metrics in log-space were: MSE – 0.1742, MAE – 0.1971, R^2 – 0.986. Operating in logarithmic space effectively stabilized the training process despite the significant variation in the original permeability values. In physical scale, the coefficient of determination was $R^2 = 0.879$, further confirming the model's ability to adequately capture global permeability trends along the samples.

Although the harmonic-mean model exhibits a lower log-MSE, this metric emphasizes relative deviations around the geometric mean. In physical units the bottleneck aggregation reduces both MAE and RMSE, indicating a closer match to the laboratory permeability over the entire dynamic range.

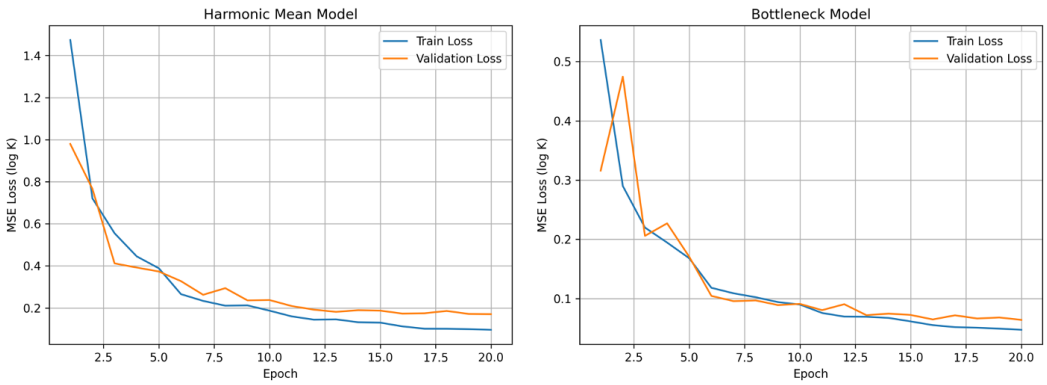

Fig. 4. Training history of the Swin models: log-MSE loss versus epoch for harmonic-mean and bottleneck cases

3.2. Model Testing Results

The prediction accuracy of the trained models was further evaluated on a test set consisting of 10 carbonate samples for which experimental gas permeability measurements were conducted (Table 1). The samples were previously scanned using microtomography, converted into stacks of slices, and preprocessed according to the methodology described earlier.

Each sample was assigned predicted permeability values generated by two models: the model trained on harmonic mean aggregation and the bottleneck model.

Table 1. Prediction results on ten new blind carbonate plugs: experimental gas permeability and Swin-predicted values from harmonic-mean and bottleneck models

Sample	Experimental gas permeability, $\mu m^2 \times 10^{-3}$	Harmonic-mean model, K3D, $\mu m^2 \times 10^{-3}$	Bottleneck model, K3D, $\mu m^2 \times 10^{-3}$
1	617.9	423.8	762.6
2	9.3	16.3	2.9
3	202.3	159.9	102.7
4	2.1	0.4	0.2
5	53.6	130.7	92.4
6	35.3	21.1	4.6
7	488.6	524.6	915.2
8	2295.2	1485.6	2336.6
9	0.4	0.1	0.2
10	984.9	1454.8	736.2

For both models, key prediction quality metrics were calculated: mean absolute error (MAE) and root mean square error (RMSE). The metrics were computed based on the absolute deviations between the predicted permeability and the experimental data. The mean absolute error for the model trained on the harmonic mean was 165.2 $\mu m^2 \times 10^{-3}$, while for the bottleneck model it was 103.9 $\mu m^2 \times 10^{-3}$. The root mean square error for these models was 303.9 $\mu m^2 \times 10^{-3}$ and 166.9 $\mu m^2 \times 10^{-3}$, respectively. Thus, the bottleneck model demonstrated significantly higher prediction accuracy: its MAE and RMSE values were 37% and 45% lower, respectively, compared to the harmonic mean model.

It is worth noting that the bottleneck model provided more stable results for both low-permeability samples (e.g., samples 4 and 9) and high-permeability samples (samples 1 and 8). In contrast, the harmonic mean model exhibited significant deviations in several high-permeability samples (e.g., errors for samples 8 and 10 reached 809.6 and 469.9 $\mu m^2 \times 10^{-3}$, respectively), although it showed relatively stable results for samples with low (samples 2, 4, and 9) and medium permeability (samples 1, 3, and 7).

Figure 5 illustrates slice-wise permeability profiles predicted by the two models for the same carbonate plug presented in Table 1 (Sample 1). The bottleneck aggregation yields a smoother profile and a closer match to the laboratory permeability (horizontal dashed line), particularly in the high-permeability intervals, whereas the harmonic-mean prediction exhibits larger local deviations. This visual comparison corroborates the statistical advantage of the bottleneck model discussed above.

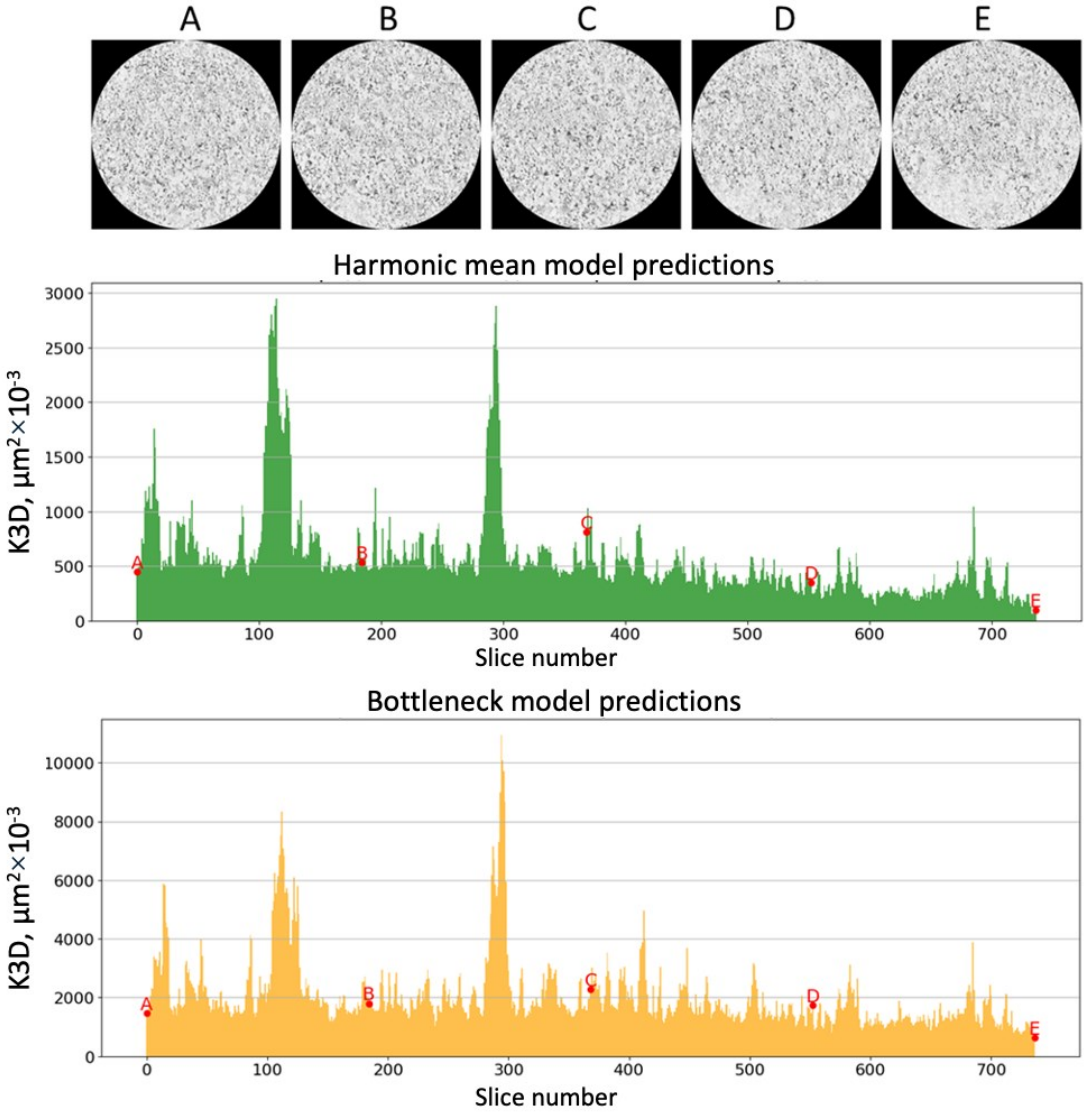

Fig. 5. Slice-wise permeability profiles predicted by the harmonic-mean and bottleneck models for a single carbonate core plug (No. 1 in Table 1)

3.3. Discussion

The two physics-guided models developed in this study demonstrate that gas permeability can be successfully estimated from stacks of low-resolution (34.6–36 μm per voxel) μCT of standard carbonate plugs. Because the Swin-Transformer architecture captures both sub-voxel textural signals and long-range connectivity, the models generalize well to heterogeneous multiscale structures that simpler convolutional approaches usually fail to handle. Inference on a complete stack takes only a few seconds, making permeability calculation a negligible addition to the digital-core workflow and allowing the results to be streamed in real time into pipelines that already perform lithofacies classification [14], porosity prediction and other physical-property assessments.

This approach is not yet universal. Slice-level labels are generated with the fractal formulation of Lei et al. [22], which begins to fail when an individual image contains a very large open fracture or cavern that behaves as an almost unlimited flow conduit. Such situations are typical of dense carbonates: one slice in the stack may show a giant void, whereas the adjacent slice is almost monolithic and impermeable. As a result, some slices receive synthetic 3-

D permeability values that are either extremely high or almost zero (up to 10^5–10^6 μm² × 10^{-3} versus < 0.1 μm² × 10^{-3}). Such a heavy-tailed distribution hampers convergence: gradients are diluted across extreme labels, and the network tends to overfit rare but scale-dominating slices. Because this issue originates from the labelling scheme rather than the network itself, plugs containing excessively large caverns or fractures are temporarily excluded from training, keeping the models within the permeability range typical of most carbonates.

A second limitation is tied to the coarse voxel size. Sub-voxel throats are blurred, sharp fracture edges appear rounded, and the minimum pore radius in the formula has to be fixed artificially. Normalization of the final values compensates for the bias in the mean, but the shape of the distribution is still significantly distorted, which limits the network's transferability to even lower resolutions or to rocks dominated by micron-scale channels.

The third issue is the absence of a trained meta-model. At present, slice-level predictions are aggregated with fixed physics-based formulas and then rescaled to match the laboratory permeability of the same standard plug. Abandoning this post-calibration in favor of a meta-aggregator would remove manual coefficient tuning, yet the data currently available are insufficient to train a secondary network without overfitting.

Among the method's strong points are the virtual absence of manual segmentation during inference, the modest size of the training set, and the ease of deployment on GPU clusters. Key directions for further development include more robust handling of extremely fractured or cavernous slices, increasing the information content of the scans through more detailed μCT acquisition modes and switching to a larger model capable of ingesting higher-resolution images, as well as broadening the diversity of the training dataset to enable subsequent training of the meta-aggregator. A realistic implementation of these steps will transform the proposed approach from a laboratory prototype into a practical tool for comprehensive digital core analysis.

4. Conclusion

The conducted study demonstrates the effectiveness of a physics-guided machine-learning approach for estimating gas permeability in carbonate reservoirs based on low-resolution μCT imagery of standard core plugs. Two Swin Transformer models were trained using permeability labels derived from a fractal analytical model and aggregated using harmonic-mean and bottleneck aggregation.

The results show that both models are capable of providing approximate, yet physically consistent, estimates of plug-scale permeability across a wide range of values. The model using bottleneck aggregation demonstrated higher overall accuracy on the test dataset, including in both low- and high-permeability intervals, which indicates its greater suitability for preliminary quantitative assessment in complex heterogeneous samples.

The harmonic-mean model also produced satisfactory results, particularly for samples with low and intermediate permeability. Due to its simplicity, this model may be useful in rapid screening scenarios or when analyzing relatively homogeneous cores with moderate permeability ranges.

A key advantage of the proposed workflow is the ability to perform inference directly on raw micro-CT slices without the need for segmentation, 3D reconstruction, or prior information about the sample geometry. This enables a significant reduction in time and labor costs associated with conventional core analysis, while maintaining compatibility with existing digital core pipelines.

The obtained results confirm the applicability of the proposed models for initial permeability screening in digital core analysis. Their integration into practical workflows can support early-stage reservoir characterization, improve efficiency in sample selection, and serve as a baseline for further development of image-based petrophysical prediction methods. Future improvements may include the implementation of a learned meta-aggregator and expansion

of the training dataset to incorporate more complex pore systems, including highly fractured and vuggy carbonates.

Acknowledgements

This paper is performed as part of the grant of the Tatarstan Academy of Sciences, provided to young candidates of science (postdoctoral fellows) for the purpose of defending their doctoral dissertation, conducting research, as well as performing their work duties in scientific and educational organizations of the Republic of Tatarstan within the framework of the State Program of the Republic of Tatarstan "Scientific and Technological Development of the Republic of Tatarstan" (Agreement No.20/2024-PD).

References

1. Tembely M., AlSumaiti A.M., Alameri W.S. Machine and deep learning for estimating the permeability of complex carbonate rock from X-ray micro-computed tomography // *Energy Reports*. 2021. Vol. 7. P. 1460–1472.
2. Wu H.Y. et al. Deep learning in the advanced core sample porosity determination with XCT image // *Earth Science Informatics*. 2025. Vol. 18, № 1. P. 17.
3. Kadyrov R., Statsenko E., Galiullin B. The porous space structure of Domanik shales in the east of Russian plate // *International Multidisciplinary Scientific Geoconference SGEM*. 2018. Vol. 18, № 1.4. P. 907–914.
4. Zhang H. et al. Influence of heterogeneity on carbonate permeability upscaling: a renormalization approach coupled with the pore network model // *Energy & Fuels*. 2022. Vol. 36, № 6. P. 3003–3015.
5. Karimpouli S., Tahmasebi P. Image-based velocity estimation of rock using convolutional neural networks // *Neural Networks*. 2019. Vol. 111. P. 89–97.
6. Karimpouli S., Kadyrov R. Multistep super-resolution Double-U-Net (SRDUN) for enhancing the resolution of Berea sandstone images // *Journal of Petroleum Science & Engineering*. 2022. Vol. 216. P. 110833.
7. McPhee C., Reed J., Zubizarreta I. *Core Analysis: A Best Practice Guide*. Developments in Petroleum Science. Vol. 64. 1st ed. Elsevier, 2015. 852 p.
8. Niya S.M.R., Selvadurai A.P.S. A statistical correlation between permeability, porosity, tortuosity and conductance // *Transport in Porous Media*. 2018. Vol. 121, № 3. P. 741–752.
9. Costa A. Permeability-porosity relationship: a re-examination of the Kozeny–Carman equation based on a fractal pore-space geometry assumption // *Geophysical Research Letters*. 2006. Vol. 33, № 2. L02318.
10. Xu P., Yu B. Developing a new form of permeability and Kozeny–Carman constant for homogeneous porous media by means of fractal geometry // *Advances in Water Resources*. 2008. Vol. 31, № 1. P. 74–81.
11. Saxena N. et al. Estimating permeability from thin sections without reconstruction: digital rock study of 3D properties from 2D images // *Computers & Geosciences*. 2017. Vol. 102. P. 79–99.
12. Karimpouli S. et al. Applicability of 2D algorithms for 3D characterization in digital rock physics: an example of a machine-learning-based super-resolution image generation // *Acta Geophysica*. 2024. Vol. 72, № 2. P. 861–874.
13. Kadyrov R.I. Multiple cubes growth algorithms for simple representative elementary volume determination on 3D binary images // Scientific Visualization. 2024. Vol. 16, № 1. P. 124–135.
14. Kadyrov R., Statsenko E., Nguyen T.H. Integrating μCT imaging of core plugs and transfer learning for automated reservoir rock characterization and tomofacies identification // *Marine & Petroleum Geology*. 2024. Vol. 168. P. 107014.

15. Zhang H. et al. Permeability prediction of low-resolution porous-media images using an autoencoder-based convolutional neural network // *Journal of Petroleum Science & Engineering*. 2022. Vol. 208. P. 109589.

16. Araya-Polo M. et al. Deep-learning-driven permeability estimation from 2D images // Computational Geosciences. 2020. Vol. 24, № 2. P. 571–580.

17. Wu J., Yin X., Xiao H. Seeing permeability from images: fast prediction with convolutional neural networks // *Science Bulletin*. 2018. Vol. 63, № 18. P. 1215–1222.

18. Alqahtani N. et al. Machine learning for predicting properties of porous media from 2D X-ray images // *Journal of Petroleum Science & Engineering*. 2020. Vol. 184. P. 106514.

19. Alqahtani N., Armstrong R.T., Mostaghimi P. Deep-learning convolutional neural networks to predict porous-media properties // *SPE Asia Pacific Oil & Gas Conference and Exhibition* (APOGCE). Kuala Lumpur, 2018. Paper SPE-191493-MS.

20. Tembely M., AlSumaiti A. Deep learning for fast and accurate prediction of complex carbonate rock permeability from 3D micro-CT images // Abu Dhabi International Petroleum Exhibition & Conference (ADIPEC). Abu Dhabi, 2019. Paper SPE-197457-MS.

21. Kalule R. et al. Stacked ensemble machine learning for porosity and absolute-permeability prediction of carbonate rock plugs // *Scientific Reports*. 2023. Vol. 13, № 1. P. 9855.

22. Lei G. et al. Estimating permeability of porous media from 2D digital images // *Journal of Marine Science & Engineering*. 2023. Vol. 11, № 8. P. 1614.

23. Meyer F. Topographic distance and watershed lines // *Signal Processing*. 1994. Vol. 38, № 1. P. 113–125.

24. Kadyrov R.I., Zakirov T.R. 2D fractal and multifractal analysis of porous space in carbonate oil reservoir // *Neftyanoye Khozyaystvo – Oil Industry*. 2016. № 11. P. 72–74.

25. Baek S.H. et al. X-ray computed micro-tomography imaging of abiotic carbonate precipitation in porous media from a supersaturated solution: insights into effect of CO_2 mineral trapping on permeability // *Water Resources Research*. 2019. Vol. 55, № 5. P. 3835–3855.

26. Bouchard J. et al. Terahertz imaging for non-destructive porosity measurements of carbonate rocks // *Scientific Reports*. 2022. Vol. 12, № 1. P. 18018.

27. Liu Z. et al. Swin Transformer: hierarchical vision transformer using shifted windows // *Proceedings of the IEEE/CVF International Conference on Computer Vision*. 2021. P. 9992–10002.